[1]Motlatsi Cletus Lehloka

[2]Zenghui Wang

Harmonics Analysis on Model Predictive Control-based Algorithm for Partial Shading Mitigation on PV Array

Journal of Electrical Systems

Abstract: - The photovoltaic (PV) systems are inherently intermittent due to unpredictable weather phenomena. The efficiency and reliability of these technologies depend solemnly on the intensity of sunlight, which, in practical conditions, is variable and varies linearly, nonlinearly, and abruptly with time. This study outlines the usual effects of power electronic devices, specifically the harmonics generated by variable switching frequencies as employed in PV arrays for partial shading mitigation. The buck converter-based model predictive control (MPC) algorithm was developed from the first principles and implemented in MATLAB/Simulink for harmonics detection on the PV array operating under various (nonlinear and linear irradiation) partial shading conditions (PSCs). The buck converter was developed to automatically inject a deficit current to curb power mismatch due to PSCs on the array. According to the simulation results, the artificial intelligence (AI) controlled converter generated a deficit current signal containing minimal to no distortion despite the mismatched PV module power due to PSCs.

Keywords: Photovoltaic (PV), model predictive control (MPC), buck converter, harmonics, cost function.

I. INTRODUCTION

The application of power converters in renewable energy technologies has become increasingly popular due to their robustness and high efficiency in energy conversion [1]. Some proposed photovoltaic (PV) partial shading effects mitigation algorithms employ boost or buck converters to curb the effects of partial shading on PV modules as suggested by the authors in [2]. Power converters are widely utilized in several applications, such as solar inverters and adjustable speed drives (ASD), due to the demands of energy-efficient appliances and the usage of renewable energy supplies [3]. Distribution networks have a sizable portion of their loads made up of ASDs. Global electrical energy consumption in low-voltage distribution grids is thought to be primarily attributed to motor drives [4], [5]. That is why new topologies, control algorithms, and rapid switching devices have been used increasingly in motor drive applications to improve these systems' efficiency and energy conservation [6]. However, producing harmonics in electrical networks is one of the primary disadvantages of ASDs [7]. These harmonics cause equipment to overheat, distribution transformers to lose power, and grid instability problems [8]. Since the proposed current injection technique for partial shading effects mitigation in [9] entails power converters that operate at various switching frequencies, undesirable high-frequency harmonics might be generated as mentioned in some literature [10], [11]. Therefore, the analysis of harmonics generated by high switching frequency power converters adopted for partial shading effects mitigation and performance optimization must be made [12]. This is because the harmonics have temporary and enduring effects on electrical equipment, and communication signaling and reduce electrical network reliability, efficiency, and power quality [13]. In addition, any grid-connected device that produces harmonics impacts other devices connected to the same grid. For example, the transformers can amplify low amplitude harmonics emissions from the low voltage side of the system to noticeable or undesirable levels in cases of grid-tied PV systems [14].

For PV systems, there has been a discussion of various power quality and operation requirements for future smart grids [15]. More research is necessary because, as mentioned in [16] and [17], more devices generate disturbances in the high-frequency range of 2-150 kHz that leads to malfunctions in the equipment. In [18], a useful measurement strategy of high-frequency harmonics up to 9 kHz is presented. Authors in [19] have suggested a method to eliminate particular current harmonics from the grid. As noted in [20], the primary difficulties in measuring high-frequency harmonics are their comparatively small magnitudes in comparison to low-frequency distortions and the need for extremely precise voltage and current sensors throughout a broad frequency range.

[1, 2] University of South Africa, Department of Electrical and Smart Systems Engineering, South Africa

Email: [1]lehlomc@unisa.ac.za, [2] wangz@unisa.ac.za

Apart from that, the proposed model predictive control-based (MPC-based) PV mitigation and optimization algorithm employs a switch-controlled buck converter that injects the required amount of current to mitigate the effects of partial shading on the PV array. Fig. 1 depicts a 2×2 PV configuration of the proposed MPC algorithm-based PV mitigation algorithm. The PV module P_{11} is partially shaded with an irradiance of 500 W/m^2 while other PV modules operate at 1000 W/m^2. The dedicated MPC-controlled buck converter is given by the green block and its respective circuit parameters are given in subsequent sections. The associated MPC controller block as simulated in MATLAB/Simulink is shown in fig. 2.

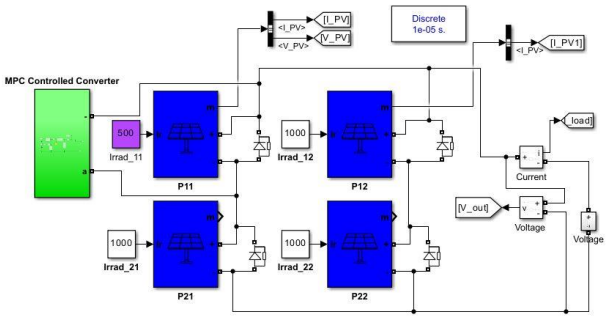

Fig. 1. Block diagram of a 2×2 PV array configuration of the proposed MPC algorithm-based PV mitigation technique

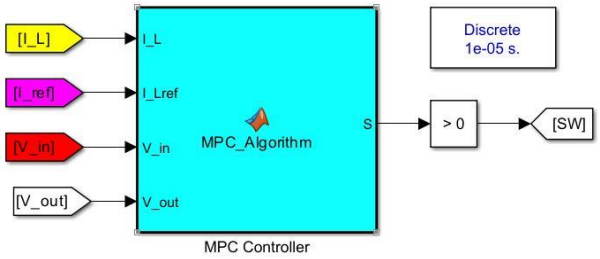

Fig. 2. An MPC algorithm block in Simulink

Since the IGBT switch position represents the actuation signal or manipulated variable in the MPC algorithm, the injected current might contain high-frequency distortions due to switching and abrupt changes in PV systems dynamics. In other conventional boost or buck converter switch control practices such as pulse width modulation (PWM), the duty cycle D ϵ [0:1] is the primary control signal [20]. Therefore, the associated harmonics can be derived and modelled from the PWM pulse pattern, and the filtering circuit can be realized to filter out unwanted harmonics [21]. The MPC algorithm tracks the reference signal by optimizing the switch position thereby generating a wide band of distortions [22]. These distortions might have unacceptable levels and can propagate throughout the system and potentially damage other system devices and equipment [9], [13]. In this regard, the distortions generated by the proposed MPC-based PV mitigation and optimization approach that utilizes a buck converter to inject deficit current to curb the effects of partial shading must be investigated.

Moreover, current measurement forms an integral part of the MPC algorithm since the measured optimal current is used as a reference signal [23]. In this regard, an extremely low noise current signal is required to ensure the accuracy of the reference signal [24]. This is because high levels of distortions in the system can severely impact digital measuring devices [25]. Authors in [26] suggest that due to the introduction of unwanted fluctuations, or ”noise”, unrelated to the phenomenon being measured, experimental data sets are never perfect. Similar to how noise can distort measurement data, it can also reduce or obscure fault patterns when sampling data using various signal processors [27].

Authors in [2] proposed a current injection method where a buck converter, as shown in fig. 3 was used on a 2×2 PV array to improve the performance of the PV array during various partial shading conditions (PSCs). The mitigation strategy worked perfectly, however, the control strategy was manually implemented and therefore, seemed impractical particularly when controlling large PV arrays under various operating conditions. According to [28] manual operations can be slower and less precise than automated methods, resulting in decreased production and efficiency. In this research, the artificial intelligence (AI) advanced control algorithm (MPC) is automated in such a way that it injects the required current to mitigate and optimize the PV array under various PSCs. AI has been widely implemented in several sectors to enhance efficiency, accuracy, and decision-making skills [29]. The integration of AI in the solar energy industry has opened up new prospects for transforming the

renewable energy sector [30]. Incorporating AI techniques and algorithms can increase solar energy systems' efficiency, productivity, and levels of performance [31]. To enhance energy capture, the buck-converter MPC-based AI algorithm finds patterns, modifies elements and optimizes the system by matching the power levels of the mismatched PV panels. The algorithm samples the best performing PV panel and then injects the deficit current from the buck converter to match the rest of the system. The regenerative power injected by the buck-converter is generally less than the output power of the system and thus the system is optimized.

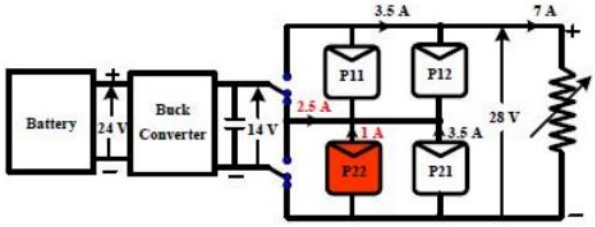

Fig. 3. The current injection method for performance for performance improvement of the PV array under different PSC [2]

II. BUCK CONVERTER MATHEMATICAL MODEL

In this section, the mathematical model for the buck converter adopted for the MPC algorithm is formulated. The dedicated circuit is shown in fig. 4 and the circuit parameters are provided in table 1. The load resistor emulates the mismatched PV module. It is worth mentioning that the switch position of the converter is controlled by the optimal ON/OFF signal from the controller. The MPC controller can be realized or rapidly prototyped through a high clock speed microcontroller device such as the STM32 32-bit ARM Cortex series from STMicroelectronics. This is because the MPC algorithm is deployable in low power and memory microcontroller (MCU) device [32], [33]. DC-DC buck converters are usually employed to lower the input voltage [34]. As a result, they are particularly favored in high-voltage power sources, such as the battery bank of a high-voltage PV system [35]. DC–DC converters are analyzed based on a few fundamental operating parameters, namely potential discontinuous conduction mode (DCM) and continuous conduction mode (CCM), the two switching states [36]. The converter's passive parts, the voltage entering the converter, and the switching frequency form the foundation for DCM and CCM operations. The control method of the converter is established for the CCM condition based on the system parameters. The buck converter only has two possible switching states, S = 1 and S = 0 where S = 1 denotes the ON position while S = 0 denotes the OFF position of the switch.

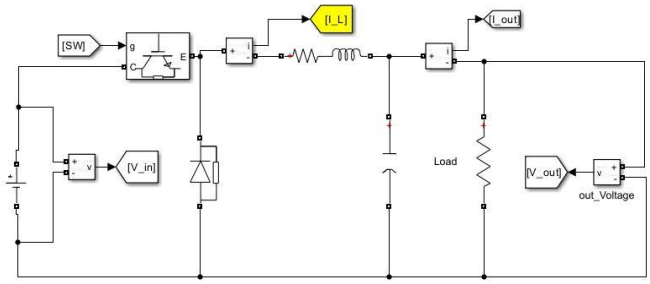

Fig. 4. A general circuit diagram of the buck converter

TABLE I: Parameters of the buck converter adopted for MPC control.

S/No	Parameter	Value
1	Sampling period (T_s)	10 µs
2	Inductor series resistance (RL)	20 mΩ
3	Inductance (L)	1 mH
4	Capacitance (C)	55 µF
5	Input voltage (V_{in})	120 V
6	Output voltage (V_{out})	29 V

Fig. 5 depicts a simplified circuit configuration of the converter when the switch is ON and fig. 6 represents the OFF state. The expression for inductor voltage for both the ON and OFF switch states are described by equations 1 and 2 respectively. These equations are derived from applying voltage laws on these circuits.

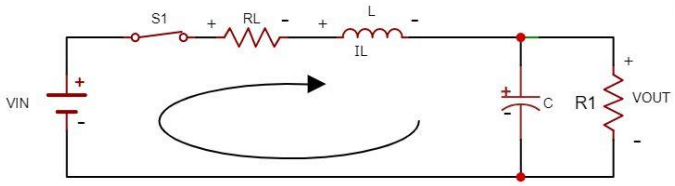

Fig. 5. A simplified equivalent circuit diagram of a buck converter when the switch is in ON state (S = 1)

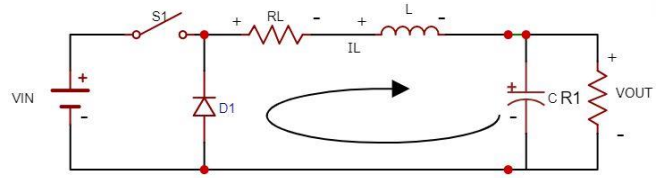

Fig. 6. A simplified equivalent circuit diagram of a buck converter when the switch is in OFF position (S = 0)

$$L\frac{dI_L}{dt} = V_{in} - V_{out} - I_L R_L \quad (1)$$

$$L\frac{dI_L}{dt} = -(V_{out} + -I_L R_L) \quad (2)$$

Where V_{in}, V_{out}, R_L, and I_L are input voltage, output voltage, inductor equivalent series resistance, and continuous time inductor current respectively. The piecewise inductor voltage functions given by equations 1 and 2 can be combined to formulate a new expression for both switch positions and is given by equation 3. It is worth noting that equation 3 can be reduced to equation 1 if S = 1 and to equation 2 when S = 0.

$$L\frac{dI_L}{dt} = V_{in}S + (V_{out} - I_L R_L)(S - 1)\,(V_{out} + I_L R_L)S \quad (3)$$

The MPC algorithm forecasts system behavior based on optimum control states and is generally derived from the continuous time plant model [37]. The next best control actuation is then chosen to minimize the cost function, taking into account the anticipated future states of the system. Depending on the type of system and performance requirements, the prediction horizon (N) can be chosen to define the cost function evaluation for each sample period [38]. Predictions are shifted one step, and the subsequent optimization is carried out when the prediction horizon is chosen to be larger than one [39]. To identify the ideal future switching state, a prediction horizon of one (N = 1) is chosen for this investigation. Consequently, the following general definition (equation 4) of a cost function can be applied to future states, reference signals, and future actions [40].

$$J = f(x)(k), u(k), \ldots \ldots \ldots \ldots u(k + N - 1) \quad (4)$$

Where x(k), u(k), and k denote discrete state variable - sampled inductor current, optimum possible manipulated variable (which is a switch state in this study) and k, is the iteration number of samples. The following three steps can be used to apply the discrete-time MPC approach to obtain the total cost function [41]:

- Modeling all potential switching states for the converter;
- Acquiring the discrete-time model for prediction at every sampling interval and
- Determining the cost functions.

The preceding section presented the first step. Various discretization techniques are employed in the literature to derive the discrete-time model as the subsequent step. Amongst them, forward-difference Euler estimation method provided by equation 5 is generally utilized in first-order systems [41].

$$\frac{dI_L}{dt} \approx \frac{I_L(k+1) - I_L(k)}{T_s} \quad (5)$$

where $I_L(k)$, $I_L(k + 1)$, and Ts are discrete instantaneous inductor current, predicted inductor current, and sampling period respectively. The predicted inductor current is obtained by combining equation 3 and 5 and is given by equation 6.

$$I_L(k + 1) = I_L(k) + \frac{T_s}{L}[V_{in}S + (V_{out} + I_L(k)R_L)(S - 1) - V_{out} + I_L(k)R_L)S]) \quad (6)$$

An entirely new set of measured data is used at each sampling interval to solve the optimization problem in equation (6) and ascertain the new state of the switch. The MPC algorithm cannot identify the ideal key state using merely predictions. The error between the reference signal and the anticipated value must also be minimized to ensure optimization. The cost function generally defined in equation 4 is employed for this purpose. In this study, the cost function is given by equation 7.

$$J_I(k + 1) = [I_L^*(k) - I_L(k + 1)]^2 \quad (7)$$

Where $I_L^*(k)$ is the measured reference inductor current obtained from an optimally operating PV module or series branch. The fixed-step control approach requires A second cost function, which forecasts the value in each sample

period and lowers the switching frequency [42]. Digital control techniques may have variable switching frequencies since they generate the switching signal without using comparators. The signal error will rise if the sample and switching frequencies are roughly equal. The cost function in equation 8 is used to reduce the switching frequency, and its impacts on the overall cost function are limited by the inclusion of a weighting factor ω. The weighting factor in this literature is set at 0.1 utilizing the cost function classification approach suggested by authors in [41].

$$J_{sw}(k+1) = \omega S(k) - S(k+1)]^2 \quad (8)$$

As previously noted, two cost functions are required to control the current and the switching frequency simultaneously. The MPC method's capability to manipulate numerous parameters in a single function is one of its primary advantages. As a result, a comprehensive cost function is produced, as indicated by equation 9 which combines Equations 7 and 8. The same strategy is utilized in this study to produce more accurate results since, as demonstrated in [41], using the squared error technique in multiple terms cost functions yields better results. The squares of equations 7 and 8 are utilized for this purpose. At each sampling time, the total cost function is computed for every conceivable switching state, and it is then minimized according to equation 10. Now that the predictive function and cost function of the MPC algorithm have been developed, the next section focuses on the implementation of the MPC algorithm for PV array partial shading mitigation.

$$J(k+1) = J_I(k+1) + J_{sw}(k+1) \quad (9)$$

$$\min J(k+1) = \min J_I(k+1) + J_{sw}(k+1) \quad (10)$$

III. MPC Algorithm for Buck Converter

The proposed MPC algorithm (cost function) is provided in Algorithm 1. The function takes the sampled inductor current $I_L(k)$, measured reference inductor current $I_L^*(k)$, converter input voltage $V_{in}(k)$, converter output voltage $V_{out}(k)$ and weighting factor ω as the inputs and returns the optimal switch state STATE as the manipulated variable of the controller. The associated flowchart for the MPC algorithm is shown in fig. 7.

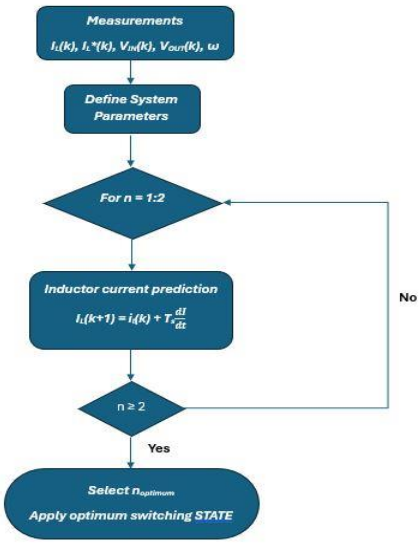

Fig. 7. Flowchart of the MPC algorithm

Algorithm 1 (MPC algorithm)

Function STATE = MPC algorithm $I_L(k), I_L^*(k), V_{in}(k), V_{out}(k)$ ω

$T_s = 10e^{-6}$;

$L = 1e^{-3}$;

$T_L = 20e^{-3}$;

$S = [1:0]$;

$J_{optimum} = \infty$;

$n_{optimum} = 1$;

persistent $S_{previous}$;

if isempty ($S_{previous}$) **do**

$S_{previous} = 0$;

End if;

for n = 1 to 2 **do**

$I_L(k+1) = I_L(k) + \frac{T_s}{L}[V_{in}S + (V_{out} + I_L(k)R_L)(S-1) - (V_{out} + I_L(k)R_L)S]$

$J_I(k+1) = [I_L^*(k) - S(k+1)(k)]^2$

$J_{sw}(k+1) = \omega[S(k) - S(k+1)(k)]^2$
$J(k+1) = J_I(k+1) + J_{sw}(k+1)$
if $(J < J_{optimum})$ **do**
$n_{optimum} = n$
$J_{optimum} = J$
end if
end for
$STATE = S(n_{optimum})$
$S_{previous} = STATE$

IV. Distortions of MPC Controlled Buck Converter

Section 1 discussed the effects of distortions in power electronic devices and electrical equipment. This section investigates these effects to ensure the safety and compliance of the MPC algorithm-based buck converter adopted for PV partial shading mitigation. The system depicted in fig. 1 is simulated in MATLAB/Simulink under linear and nonlinear system operating conditions. The irradiance of PV module P_{11} is varied, emulating both the nonlinear and linear response of the system. Fig. 8 shows the varying irradiation on P_{11}. Region 1 simulates the nonlinear behavior of the PSC while regions 2 and 3 emulate the linear response of the system when irradiance increases linearly and under constant irradiation operating conditions. Since PV module P_{12}, P_{21} and P_{22} are bombarded with constant irradiation of 1000 W/m^2 and the current from P_{12} and P_{22} series branch serves as a reference signal, the MPC algorithm controlled buck converter inject deficit current to curb power mismatch due to PV module P_{11}. Fig. 9 shows the system response in terms of load voltage. It is worth noting that the system's output voltage remains essentially constant despite variations in P_{11} irradiation. Thus, the effects of partial shading are effectively mitigated. Moreover, fig. 10 depicts the load current, inductor current, and reference signal. The reference signal is generated by taking the difference of P_{12} and P_{11}, thus the system is matched.

The inductor current tracks the reference signal without generating any overshoot and appreciable noise levels as depicted in fig. 10. This implies that the MPC-controlled buck converter generates minute levels of noise and the associated harmonics due to switching are negligible. The continuous frequency magnitude spectrum (in dB scale) of load current is shown in fig. 11 and the associated harmonics which can be regarded as noise can be seen. The dB scale as opposed to the linear scale is utilized to reveal minute higher frequency components of the load current when the PV system operates under erratic operating conditions. From the load current spectrum, the DC term emerges as the dominating component, and two relatively significant frequencies with negligible levels are seen at 2.5 kHz and 5 kHz respectively. The magnitude of these higher frequency terms are in the order of -59.67 dB and -73.16 dB at 2.5 kHz and 5.0 kHz. This implies that all associated harmonics are negligible and noise levels are extremely low, therefore, the MPC-controlled buck converter does not generate problematic distortions.

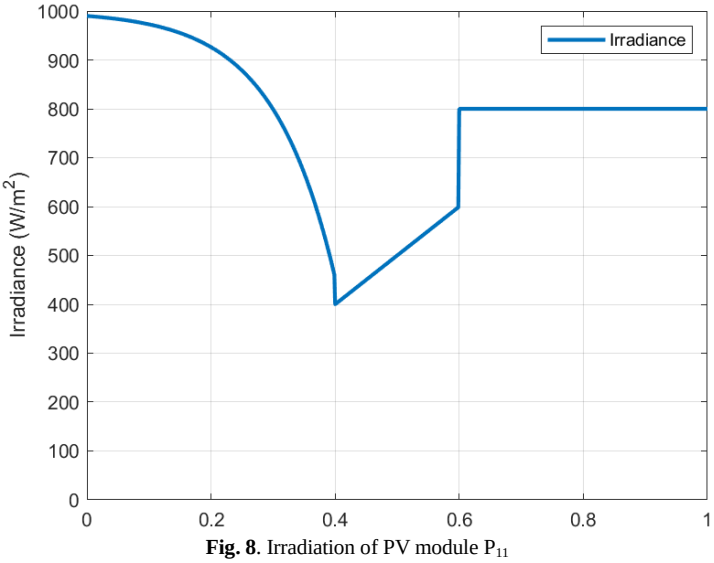

Fig. 8. Irradiation of PV module P_{11}

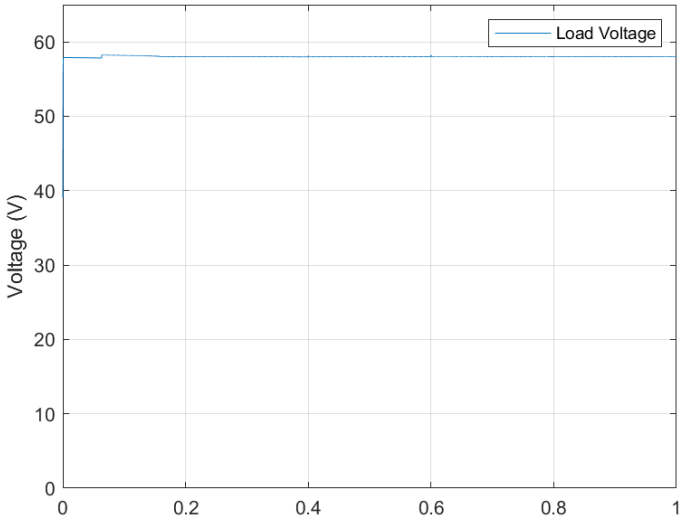

Fig. 9. Output voltage of the system

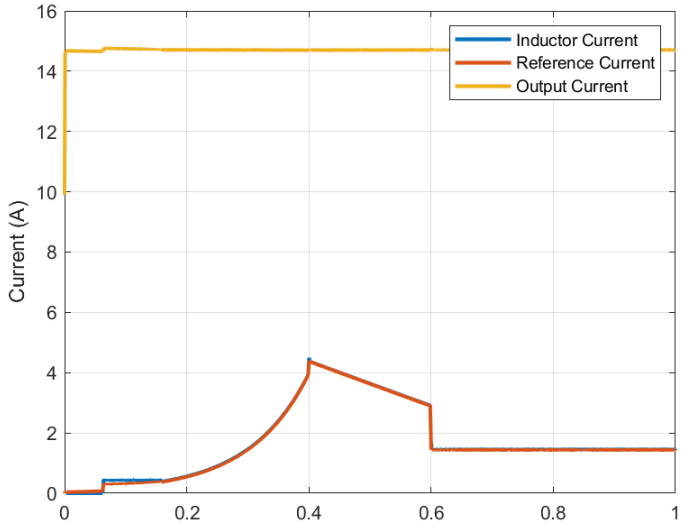

Fig. 10. Simulation results of current signals

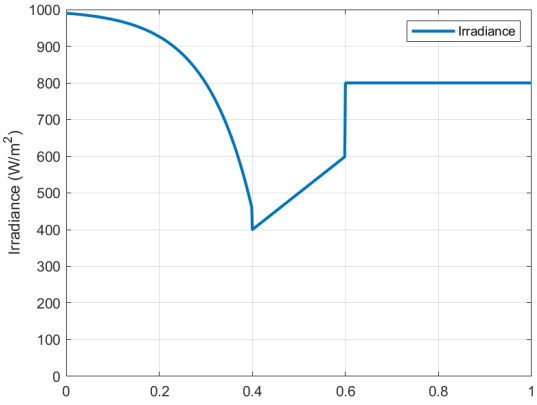

Fig. 11. The load current spectrum

V. CONCLUSION

This paper reviewed the typical impacts of power electronic devices particularly the harmonics generated by variable switching frequencies as applied in PV array partial shading mitigation. The proposed MPC algorithm-based PV mitigation approach was presented and the MPC algorithm was derived from the first principles and implemented in MATLAB/Simulink. From the simulation results, the output current and the converter-generated deficit current signal had minute noise and little to no harmonics despite having the mismatched PV module P_{11} operating under erratic operating conditions emulating practical situations. The continuous frequency magnitude spectrum of the load current, which comprises the buck converter-generated current and PV-generated current is

depicted and analyzed to investigate the distortions and noise levels present. The simulation results revealed that high-frequency components of the load current have relatively minute magnitudes and distinct frequency points are DC and small signals at 2.5KHz and 5.0KHz with magnitudes of -59 dB and -73 dB respectively. This implies that further filtering of the signal is unnecessary as the generated current signal can be regarded as smooth albeit the system was subject to abrupt operating conditions. The major contributions of this paper are:

1) Automatic control of buck converter using MPC algorithm to mitigate PV partial shading effects;
2) Application of MPC-algorithm for PV array optimization and
3) Investigation of harmonics and noise levels generated by the MPC-controlled buck converter for partial shading mitigation.

Although the discussion focused on a 2×2 PV array, extending the application to large arrays of multiple PV modules lumped together is imperative. It is also imperative to test the application in a real-world setup to validate the simulation results.

ACKNOWLEDGMENT

The author wishes to acknowledge the National Natural Science Foundation of China (Grant No. 62103298), the South African National Research Foundation (Grant Nos. AJCR230704126719 and 137951), and the South African Eskom Tertiary Education Support Programme.

REFERENCES

[1] A. Ganguly, P. K. Biswas, C. Sain, and T. S. Ustun, "Modern dc–dc power converter topologies and hybrid control strategies for maximum power output in sustainable nanogrids and picogrids—a comprehensive survey," Technologies, vol. 11, pp. 102, 2023.

[2] D. P. Winston, S. Kumaravel, B. P. Kumar, and S. Devakirubakaran, "Performance improvement of solar pv array topologies during various partial shading conditions," Solar Energy, vol. 196, pp. 228–242, 2020.

[3] F. H. Gandoman, A. Ahmadi, A. M. Sharaf, P. Siano, J. Pou, B. Hredzak, and V. G. Agelidis, "Review of facts technologies and applications for power quality in smart grids with renewable energy systems," Renewable and sustainable energy reviews, vol. 82, pp. 502–514, 2018.

[4] A. M. Haidar, K. M. Muttaqi, and D. Sutanto, "Technical challenges for electric power industries due to gridintegrated electric vehicles in low voltage distributions: A review," Energy Conversion and Management, vol. 86, pp. 689–700, 2014.

[5] T. Dragicevic, J. C. Vasquez, J. M. Guerrero, and D. Skrlec, "Advanced lvdc electrical power architectures and microgrids: A step toward a new generation of power distribution networks," IEEE Electrification Magazine, vol. 2, pp. 54–65, 2014.

[6] X. Yuan, I. Laird, and S. Walder, "Opportunities, challenges, and potential solutions in the application of fastswitching sic power devices and converters," IEEE Transactions on Power Electronics, vol. 36, pp. 3925– 3945, 2020.

[7] A. Kalair, N. Abas, A. R. Kalair, Z. Saleem, and N. Khan, "Review of harmonic analysis, modeling and mitigation techniques," Renewable and Sustainable Energy Reviews, vol. 78, pp. 1152–1187, 2017.

[8] J. Yaghoobi, F. Zare, T. Rehman, and H. Rathnayake, "Analysis of high frequency harmonics in distribution networks: 9–150 khz," in 2019 IEEE International Conference on Industrial Technology (ICIT), Feb. 2019, pp. 1229–1234, DOI: 10.1109/ICIT.2019.8755071.

[9] M. Bollen, S. Ronnberg, F. Zavoda, R. Langella, S. Djo- ¨ kic, P. Cuifo, J. Meyer, and V. Cuk, "Consequences of smart grids for power quality: Overview of the results from cigre joint working group c4. 24/cired," IEEE PES innovative smart grid technologies conference Europe (ISGT-Europe), Sep. 2017, pp. 1–6, IEEE, 2017, DOI: 10.1109/ISGTEurope.2017.8260116.

[10] P. De Rua, T. Roose, O. C. Sakinci, N. d. M. D. Campos, ¨ and J. Beerten, "Identification of mechanisms behind converter-related issues in power systems based on an overview of real-life events," Renewable and Sustainable Energy Reviews, vol. 183, pp. 113431, 2023.

[11] I. Dewayalage, D. A. Robinson, S. Elphick, and S. Perera, "Measurement of high-frequency voltage harmonics above 2 khz in high-voltage networks," Energies, vol. 17, p. 892, 2024.

[12] D. Mathew, J. P. Ram, and Y.-J. Kim, "Unveiling the distorted irradiation effect (shade) in photovoltaic (pv) power conversion–a critical review on causes, types, and its minimization methods," Solar Energy, vol. 266, p. 112141, 2023.

[13] M. Bollen, M. Olofsson, A. Larsson, S. Ronnberg, and ¨ M. Lundmark, "Standards for supraharmonics (2 to 150 khz)," IEEE Electromagnetic Compatibility Magazine, vol. 3, pp. 114–119, 2014.

[14] S. Sepasi, C. Talichet, and A. S. Pramanik, "Power quality in microgrids: A critical review of fundamentals, standards, and case studies," IEEE Access, vol. 11, pp. 108493-108531, 2023

[15] S. Ronnberg and M. Bollen, “Power quality issues in ¨ the electric power system of the future,” The electricity journal, vol. 29, pp. 49–61, 2016.
[16] T. Rehman, J. Yaghoobi, and F. Zare, “Harmonic issues in future grids with grid connected solar inverters: 0–9 khz,” in 2018 Australasian Universities Power Engineering Conference (AUPEC), Nov. 2018, pp. 1–6, DOI: 10.1109/AUPEC.2018.8757979.
[17] A. Alduraibi, J. Yaghoobi, F. Zare, and R. Sharma, “A new technology to reduce harmonic emission in distribution networks: Addressing iec 61000-3-12,” Australasian Universities Power Engineering Conference (AUPEC), Nov. 2018, pp. 1–6, DOI: 10.1109/AUPEC.2018.8758007.
[18] D. Amaripadath, R. Roche, L. Joseph-Auguste, D. Istrate, D. Fortune, J.-P. Braun, and F. Gao, “Power quality disturbances on smart grids: Overview and grid measurement configurations,” in 2017 52nd International Universities Power Engineering Conference (UPEC), Dec, 2017, pp. 1–6, DOI: 10.1109/UPEC.2017.8231975.
[19] F. Mendez-Diaz, B. Pico, E. Vidal-Idiarte, J. Calvente, and R. Giral, “Hm/pwm seamless control of a bidirectional buck–boost converter for a photovoltaic application,” IEEE Transactions on Power Electronics, vol. 34, pp. 2887–2899, 2018.
[20] J. K. Motwani, Y. Xue, A. Nazari, D. Dong, I. Cvetkovic, and D. Boroyevich, “Modeling of power electronics systems and pwm modulators in harmonic-state space,” IEEE Open Journal of Power Electronics, vol. 3, pp. 689–704, 2022.
[21] A. Cataliotti, V. Cosentino, G. Crotti, A. Delle Femine, D. Di Cara, D. Gallo, D. Giordano, C. Landi, M. Luiso, M. Modarres, et al., “Compensation of nonlinearity of voltage and current instrument transformers,” IEEE Transactions on Instrumentation and Measurement, vol. 68, pp. 1322–1332, 2018.
[22] I. Harbi, J. Rodriguez, E. Liegmann, H. Makhamreh, M. L. Heldwein, M. Novak, M. Rossi, M. Abdelrahem, M. Trabelsi, M. Ahmed, et al., “Model predictive control of multilevel inverters: Challenges, recent advances, and trends,” IEEE Transactions on Power Electronics, vol. 38, pp. 10845– 10868, 2023.
[23] R. Marimuthu et al., “Review on advanced control techniques for microgrids,” Energy Reports, vol. 10, pp. 3054–3072, 2023.
[24] Z. Wang, Y. Du, K. Wei, K. Han, X. Xu, G. Wei, W. Tong, P. Zhu, J. Ma, J. Wang, et al., “Vision, application scenarios, and key technology trends for 6g mobile communications,” Science China Information Sciences, vol. 65, pp. 151301, 2022.
[25] U. Doll, M. Migliorini, J. Baikie, P. K. Zachos, I. Rohle, ¨ S. Melnikov, J. Steinbock, M. Dues, R. Kapulla, D. G. MacManus, et al., “Non-intrusive flow diagnostics for unsteady inlet flow distortion measurements in novel aircraft architectures,” Progress in Aerospace Sciences, vol. 130, pp. 100810, 2022.
[26] H. Ehya, T. N. Skreien, A. Nysveen, and R. Nilssen, “The noise effects on signal processors used for fault detection purpose,” in 2020 23rd International Conference on Electrical Machines and Systems (ICEMS), Nov. 2020, pp. 183–188, DOI: 10.23919/ICEMS50442.2020.9290831.
[27] F. Alharbi, S. Luo, H. Zhang, K. Shaukat, G. Yang, C. A. Wheeler, and Z. Chen, “A brief review of acoustic and vibration signal-based fault detection for belt conveyor idlers using machine learning models,” Sensors, vol. 23, pp. 1902, 2023.
[28] F. Iqbal, S. Ahmed, F. Amin, S. Qayyum, and F. Ullah, “Integrating bim–iot and autonomous mobile robots for construction site layout printing,” Buildings, vol. 13, pp. 2212, 2023.
[29] A. Al-Surmi, M. Bashiri, and I. Koliousis, “Ai based decision making: combining strategies to improve operational performance,” International Journal of Production Research, vol. 60, pp. 4464–4486, 2022.
[30] Z. Liu, Y. Sun, C. Xing, J. Liu, Y. He, Y. Zhou, and G. Zhang, “Artificial intelligence powered large-scale renewable integrations in multi-energy systems for carbon neutrality transition: Challenges and future perspectives,” Energy and AI, vol. 10, pp. 100195, 2022.
[31] F. Alassery, A. Alzahrani, A. I. Khan, K. Irshad, and S. Islam, “An artificial intelligence-based solar radiation prophesy model for green energy utilization in energy management system,” Sustainable Energy Technologies and Assessments, vol. 52, pp. 102060, 2022.
[32] Y. Li, S. E. Li, X. Jia, S. Zeng, and Y. Wang, “Fpga accelerated model predictive control for autonomous driving,” Journal of intelligent and connected vehicles, vol. 5, pp. 63–71, 2022.
[33] D. G. Nguyen, S. Park, J. Park, D. Kim, J. S. Eo, and K. Han, “An mpc approximation approach for adaptive cruise control with reduced computational complexity and low memory footprint,” IEEE Transactions on Intelligent Vehicles, vol. 9, pp. 3154-3167, 2023.
[34] U. Nasir, Z. Iqbal, M. Rasheed, and M. Bodla, “Voltage mode controlled buck converter under input voltage variations,” in 2015 IEEE 15th International Conference on Environment and Electrical Engineering (EEEIC), July, 2015, pp. 986–991, DOI: 10.1109/EEEIC.2015.7165298.
[35] S. Ghosh, U. Bhattacharjee, S. Bhowmik, and D. S. K. Martha, “A review on high-capacity and high-voltage cathodes for next-generation lithium-ion batteries,” Journal of Energy and Power Technology, vol. 4, pp. 1– 77, 2022.
[36] E. Irmak and N. Guler, “A model predictive control-based ¨ hybrid mppt method for boost converters,” International Journal of Electronics, vol. 107, pp. 1–16, 2020.

[37] A. Norouzi, H. Heidarifar, H. Borhan, M. Shahbakhti, and C. R. Koch, "Integrating machine learning and model predictive control for automotive applications: A review and future directions," Engineering Applications of Artificial Intelligence, vol. 120, pp. 105878, 2023.

[38] H. Li and Q. Wei, "Data-driven optimal control for half-vehicle suspension system via adaptive dynamic programming," in 2022 IEEE 11th Data Driven Control and Learning Systems Conference (DDCLS), Aug. 2022, pp. 525– 530, DOI: 10.1109/DDCLS55054.2022.9858476.

[39] A. Zhukov and V. Diachenko, "The autonomous underwater vehicle adaptive control algorithm based on particle filter," in 2019 4th International Conference on Robotics and Automation Engineering (ICRAE), Nov. 2019, pp. 45– 49, DOI: 10.1109/ICRAE48301.2019.9043829.

[40] M. Metry, M. B. Shadmand, R. S. Balog, and H. AbuRub, "Mppt of photovoltaic systems using sensorless current-based model predictive control," IEEE Transactions on Industry Applications, vol. 53, pp. 1157– 1167, 2016.

[41] J. Rodriguez and P. Cortes, Predictive control of power converters and electrical drives. John Wiley & Sons, 2012.

[42] M. Danandeh et al., "Comparative and comprehensive review of maximum power point tracking methods for pv cells," Renewable and Sustainable Energy Reviews, vol. 82, pp. 2743–2767, 2018.

[43] M. Danandeh et al., "Comparative and comprehensive review of maximum power point tracking methods for pv cells," Renewable and Sustainable Energy Reviews, vol. 82, pp. 2743–2767, 2018.